Cite this as: Cryst. Growth Des. 2014, 14, 5585−5592

dx.doi.org/10.1021/cg500833s |

Gas Adsorption, Magnetism and Single-Crystal to Single-Crystal Transformation Studies of a Three-Dimensional Mn(II) Porous Coordination Polymer

Rashmi A. Agarwal,[a] *Soumya Mukherjee*,[b] *E. Carolina Sañudo,*[c] *Sujit K. Ghosh*[b] *and Parimal K. Bharadwaj*[a]*

[a]*Department of Chemistry, Indian Institute of Technology Kanpur, 208016, India*

[b] *Department of Chemistry, Indian Institute of Science Education and Research (IISER), Dr. Homi Bhabha Road, Pashan, Pune, Maharashtra 411021, India*

[c]*Departament de Quımica Inorganica, Universitat de Barcelona, Diagonal, 645, 08028-Barcelona, Spain*

Abstract. A porous coordination polymer $\{[Mn_2(DBIBA)_3]\cdot(NO_3)\cdot 3DMF\cdot 4H_2O\}_n$ (**1**) [DBIBAH = 3,5-di(1H-benzo[d]imidazol-1-yl)benzoic acid] has been synthesized solvothermally and structurally characterized by single-crystal X-ray diffraction. This compound shows significant selective CO_2 uptake at low temperature. **1** exhibits antiferromagnetic properties below 17 K, confirmed by magnetic susceptibility measurements. Four new coordination polymers: $\{[Mn_2(DBIBA)_3]\cdot ClO_4\cdot 3DMF\cdot 3H_2O\}_n$ (**2**), $\{[Mn_2(DBIBA)_3]\cdot Cl\cdot DMF\cdot H_2O\}_n$ (**3**), $\{[Mn_2(DBIBA)_3]\cdot NO_3\cdot CH_3OH\cdot 7H_2O\}_n$ (**4**) and $\{[Mn_2(DBIBA)_3]\cdot NO_3\cdot 2CH_3COCH_3\cdot H_2O\}_n$ (**5**), have been synthesized from **1** via anion/solvent exchange protocols at room temperature.

Introduction

Studies on the functional aspects of porous metal-organic framework materials such as ion exchange, [1] separation, [2] gas storage, [3] sensor[2,4] and magnetism[4,5] are rapidly emerging. A large number of highly porous MOFs have been synthesized which are capable of storing huge amount of CO_2, as well as significant amounts of other gases.[6] Separation of CO_2 from other gases have high technological and industrial importance.[7] Ability to synthesize MOFs with

various organic linkers and metal nodes provides tremendous flexibility in tailoring the porous material to acquire specific physical characteristics and chemical functionalities. For an effective optimized adsorption of CO_2, a periodic porous structure is desirable where uptake and release are fully reversible and flexible, by which chemical functionalization and molecular level fine-tuning can be attained.[8] Meanwhile, carboxylate bridged Mn(II) species are of particular interest, since such systems are known to exist at the active centers of some Mn(II) containing enzymes.[9] Besides, high spin Mn(II) contain up to five unpaired electrons; thus the assembly with multicarboxylate is seemingly inclined to the formation of large clusters and extended solids.[10,11] Bulk magnetic properties mainly depend on the bridging modes and the bridging geometry. In recent years, various cyanide, azides, nitrogen-containing aromatic ligands, or carboxylates have been primarily used for the design of hybrid metal-organic compounds with interesting magnetic properties.[12] A great deal of work is essential to understand the underlying structural features, that govern the exchange coupling between paramagnetic centres, since such a relationship is complex and has so far remained elusive.[13] Self-assembly and its fascinating progress have been highly influenced by several factors, such as the varying counter-ions, temperature and solvent, in addition to the nature of metal/ligand.[14] Anion exchange has attracted increasing attention in recent years, because it opens up novel avenues to constitute such frameworks potentially attractive as anion exchange materials.[15,16] When the framework-open space is occupied by molecular guests, the existing interactions between the host-framework and these guest species are expected to provide useful relationships between the concerned structure and gas sorption properties.[17] Single-crystal to single-crystal transformation is extremely desirable owing to the systematic study of gas storage and separation, since it allows exact monitoring of how the crystal structure, location and orientation of guest molecules in the voids is changing during transformation process in the crystalline phase.[18] This can be potentially important to in using the coordination space for

applications.[19] Herein, we report the synthesis, structural characterization, gas sorption and magnetic properties of a 3D-coordination polymer $\{[Mn_2(DBIBA)_3]\cdot(NO_3)\cdot 3DMF\cdot 4H_2O\}_n$ (**1**), synthesized by utilizing a bifurcated ligand consisting of benzimidazole moieties as N donor centres and carboxyl group as O donor centres (Scheme 1). The linker is particularly chosen because there is the possibility of rotation about the C—N bond that can allow cooperative movement of the metal-linker ensemble necessary for single-crystal to single-crystal (SCSC) transformations. Complex **1** affords four new coordination polymers (**2**–**5**) via anion/solvent induced SCSC transformations.

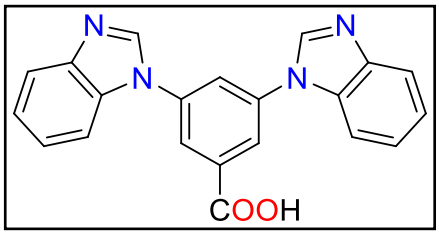

Scheme 1. Representation of the ligand 3,5-di(1H-benzo[d]imidazol-1-yl)benzoic acid (DBIBAH)

Experimental Section

Materials. Reagent grade 3,5-difluorobenzonitrile and metal salts were acquired from Aldrich and used as received. All solvents, benzimidazole and K_2CO_3 were procured from S. D. Fine Chemicals, India. Solvents were purified prior to use following standard protocols.

Physical Measurements. Infrared spectra were recorded (KBr disk, 400-4000 cm^{-1}) using a Perkin-Elmer equipment model spectrum version II. ^1H NMR spectra were recorded on a JEOL-ECX 500 FT (500 MHz) in DMSO-d_6 with Me_4Si as the internal standard. ESI mass spectra were recorded on a WATERS Q-TOF premier mass spectrometer. Thermogravimetric analysis data plots were recorded using a Mettler Toledo (heating rate of 5 ^oC/min) TGA instrument. Powder X-ray diffraction (CuK_α radiation, scan rate 3^o/min, 293 K) was performed on a Bruker D8 Advance Series 2 powder X-ray diffractometer. Low pressure gas sorption

measurements were performed using BelSorpmax (Bel Japan). All the gases used were of 99.999% purity. As-synthesized compound **1** was heated at 160 °C under vacuum for 10 h, to get guest free compound. Prior to adsorption measurement, the guest free sample was pre-treated at 160 °C under vacuum for 4 h, using BelPrepvacII, and purged with He on cooling. Between the experiments with various gases, the out-gassing procedure was repeated for *ca*. 5 h. For low temperature measurements, N_2 and H_2 adsorption isotherms were monitored at 77 K, while CO_2 gas sorption isotherm was monitored at 195 K. The adsorption isotherms at 298 K were monitored individually for the gases, namely CO_2, N_2, H_2 and CH_4. CO_2 gas sorption isotherm was also measured at 273 K. Surface area and pore size distribution were calculated using BelMaster analysis software package. Magnetic measurements were carried out in the Unitat de Mesures Magnetiques (Universitat de Barcelona) on polycrystalline samples (ca. 30 mg) with a Quantum Design SQUID MPMS-XL magnetometer equipped with a 5 T magnet. Diamagnetic corrections were calculated using Pascal's constant[19] and an experimental correction factor for the sample holder was applied.

Synthesis of 3,5-di(1H-benzo[d]imidazol-1-yl)benzoic acid (DBIBAH). In the first step, 5-di(1H-benzo[d]imidazol-1-yl)benzonitrile (DBIBN) was synthesized as previously reported.[20] In the second step, a mixture of DBIBN (2 g, 5.9 mmol) was hydrolyzed by refluxing it with an ethanolic solution of NaOH (0.35 g, 8.8 mmol) for 10 h. Finally, the resulting solution was carefully neutralized with dilute HCl to obtain a pale yellow precipitate. It was collected by filtration, washed thoroughly with water and air dried (Scheme 1). Yield: 1.8 g (90%). Melting point: 250 °C (uncorrected); IR(cm^{-1}, KBr pellet): 3403(m), 3086(m), 2421(w), 1895(w), 1704(w), 1645(w), 1605(s), 1501(s), 1473(s), 1396(w), 1244(s), 1213(s), 1167(s), 1135(m), 1091(w), 896(w), 853(w), 782(m), 761(m), 731(s), 690(m), 622(w), 542(w), 489(w), 466(w), 427(w) (Figure S1, Supporting Information). ^{1}H-NMR (DMSO-d_6, 500 MHz) δ (ppm): 8.74 (s, 2H; H_{Ar}), 8.23 (d, 3H; H_{Ar}), 7.77 (m, 4H; H_{Ar}), 7.34 (m, 4H, H_{Ar}) (Figure S2, Supporting

Information); ^{13}C NMR (DMSO-d_6) δ (ppm): 166.30, 144.21, 144.06, 138.17, 134.91, 133.26, 124.48, 123.49, 123.36, 123.08, 120.57, 111.35 (Figure S3, Supporting Information). ESI-MS: m/z [M-1] 353.10 (100%); calculated 354.13 (Figure S4, Supporting Information); Anal. calcd. for $C_{21}H_{14}N_4O_2$ (354.13): C, 71.16; H, 3.98; N, 15.82%. Found: C, 70.91; H, 4.07; N, 15.52%.

Synthesis of {[Mn_2(DBIBA)$_3$]·NO_3·3DMF·4H_2O}$_n$ (**1**). A mixture containing $Mn(NO_3)_2·4H_2O$ (0.058 g, 0.22 mmol), DBIBAH (0.04 g, 0.11 mmol) in DMF:H_2O (4 mL, 3:1 v/v) was placed in a Teflon-lined stainless steel autoclave and heated to 80 ^oC for 2 days under autogenous pressure. Then it was allowed to cool to room temperature at the rate of 1 ^oC/min. Small light brown crystals of **1** were collected in ~52% yield. The crystals were repeatedly washed with ethanol and air-dried. Anal. calcd. for $C_{72}H_{68}N_{16}O_{16}Mn_2$: C, 56.75; H, 4.50; N, 14.72%. Found: C, 56.22; H, 4.65; N, 14.82%. IR (cm^{-1}, KBr pellet): 3436(m), 3091(m), 3065(m), 2848(w), 2926(w), 1664(s), 1644(s), 1596(s), 1584(s), 1500(s), 1474(s), 1448(m), 1407(s), 1377(s), 1321(m), 1306(s), 1291(s), 1241(s), 1224(s), 1170(m), 1151(m), 1142(m), 1094(m), 1062(w), 1009(w), 906(m), 872(m), 793(m), 780(s), 766(s), 755(s), 721(s), 689(m), 657(w), 626(w), 610(w), 562(w), 520(w) (Figure S5, Supporting Information).

Synthesis of {[Mn_2(DBIBA)$_3$]·ClO_4·3DMF·3H_2O}$_n$ (**2**). Crystals of **1** were immersed in 3M aqueous solutions of $NaClO_4$ for one week at room temperature, upon which **2** was obtained without losing crystallinity. Anal. calcd. for $C_{72}H_{66}N_{15}O_{16}ClMn_2$: C, 56.02; H, 4.28; N, 11.67%. Found: C, 56.4; H, 4.5; N, 11.8%. IR (cm^{-1}, KBr pellet): 3539(m), 3093(m), 1696(m), 1663(m), 1645(s), 1596(s), 1585(s), 1502(s), 1409(s), 1378(s), 1307(s), 1291(s), 1242(s), 1225(s), 1092(s), 765(s), 755(s) (Figure S12).

Synthesis of {[Mn_2(DBIBA)$_3$]·Cl·DMF·H_2O}$_n$ (**3**). Crystals of **1** were immersed in 3M aqueous solutions of NaCl for one week at room temperature to obtain **3** without losing crystallinity. Anal. calcd. for $C_{66}H_{48}N_{13}O_8ClMn_2$: C, 61.09; H, 3.70; N, 14.03%. Found: C,

61.53; H, 3.78; N, 14.27%. IR (cm^{-1}, KBr pellet): 3417(m), 3067(m), 1663(s), 1643(s), 1595(s), 1499(s), 1404(s), 1375(s), 1241(s), 743(s) (Figure S13).

Synthesis of $\{[Mn_2(DBIBA)_3]\cdot NO_3\cdot CH_3OH\cdot 7H_2O\}_n$ (4). Crystals of **1** were dipped in dry methanol for four days to obtain **4** without losing crystalinity. Anal. calcd. for $C_{64}H_{57}N_{13}O_{17}Mn_2$: C, 55.25; H, 4.10; N, 13.09%. Found: C, 55.64; H, 4.18; N, 13.24%. IR (cm^{-1}, KBr pellet): 3370(s), 3117(s), 3067(s), 1644(s), 1598(s), 1585(s), 1501(s), 1403(s), 1367(s), 1220(s), 1171(s), 1050(s), 1011(s), 906(s), 882(s), 794(s), 781(s), 746(s), 719(s), 426(s) (Figure S14).

Synthesis of $\{[Mn_2(DBIBA)_3]\cdot NO_3\cdot 2CH_3COCH_3\cdot H_2O\}_n$ (5). Crystals of **1** were dipped in dry acetone for four days to obtain **5** in a SCSC transformation. Anal. calcd. for $C_{69}H_{53}N_{13}O_{12}Mn_2$: C, 60.63; H, 3.95; N, 13.32%. Found: C, 60.9; H, 4.11; N, 13.62 %. IR (cm^{-1}, KBr pellet): 3118(m), 1698(w), 1723(w), 1643(s), 1596(s), 1585(s), 1501(s), 1474(s), 1460(s), 1451(s), 1368(s), 1304(s), 1293(s), 1241(s), 1220(s), 1171(m), 1149(m), 1141(m), 1107(m), 906(m), 873(m), 794(m), 781(s), 764(s), 744(s) (Figure S15).

Single Crystal X-ray Studies. Single crystal X-ray data for complexes **1-5** were collected at 100 K on a Bruker SMART APEX CCD diffractometer using graphite-monochromated MoK_α radiation (λ = 0.71073 Å) as described earlier.[20] Squeeze refinement have been performed for **2–4** complexes using PLATON. For compound **5** acetone molecules were located but water molecules could not be located. Contributions from all atoms of the solvent molecules have been incorporated in both the empirical formulae and formula-weights as shown in the crystal and structure refinement data Table. In **1**, all water molecules, nitrate anion and atoms O8, N9, C37, C38, and C39 while in **4**, atoms C12, C13 and C20 were refined isotropically. Hydrogens could not be located in the difference maps for the three lattice water molecules and a distorted DMF molecule in **1**. Several DFIX and DANG commands were given for nitrate anion of **1** to fix bond distances and bond angles. To fix bond distance of perchlorate anion in **3** and between

C9 and C10, C7 and C12 in **4**, DFIX commands were given. The crystal and refinement data are collected in Table 1 and 2, while selective bond angles and bond distances are given in Table S1 in the Supporting Information.

Space for Tables 1 and 2

Results and discussion

Complex **1** was synthesized under solvothermal condition at 80 ^{o}C by utilizing DBIBAH ligand. Once isolated, it is found to be stable in air and insoluble in common organic solvents. Single crystal X-ray diffraction analysis reveals that **1** crystallizes in the monoclinic space group *C*2/*c* and the asymmetric unit consists one Mn(II) ion, 1.5 DBIBA ligand, one nitrate anion with half occupancy, one lattice water molecule with full occupancy and two free water molecules with half occupancy, one non-coordinated DMF molecule with full occupancy and

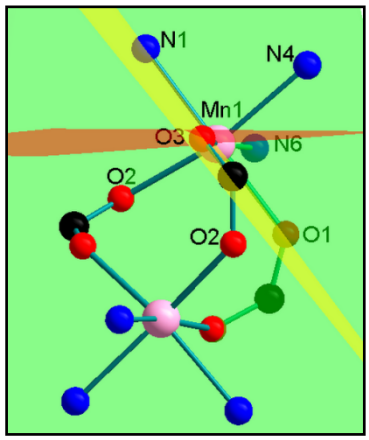

Figure 1 Showing selected planes (N1 Mn1 O1, N4 Mn1 O2 and N6 Mn1 O3) in **1**.

another DMF molecule with half occupancy. This DMF molecule is distorted and having translational symmetry passing through its nitrogen atom. **1** is iso-structural to previously reported coordination polymers of Ni(II)[21], Co(II)[20] and Mn(II)[21]; but bond angles, torsional angles and dihedral angles (Figure 1) for **1** vary considerably compared to the reported Mn(II) coordination polymer. Dihedral angle between the two planes of N1 Mn1 O1 and N6 Mn1 O3 is 56.25º, between N1 Mn1 O1 and N4 Mn1 O2 is 81.7º, while that between N4 Mn1 O2 and

N6 Mn1 O3 is 86.8º. Torsion angles N1–Mn1–O1–C1, N4–Mn1–O2–C23 and N6–Mn1–O3–C23 are -78.9º, 104.7º and -51.2º respectively. Along the crystallographic *c* axis, 1D channels of diameter ~5.8 Å (considering van der Waals radii) are present revealing strong π–π interactions between two benzene rings of two different benzimidazole moieties. Between the two benzene rings of different ligands, DMF molecules are located (Figure 2a). In the centre of the cavity, four nitrate anions with six water molecules are present (Figure 2c). These water molecules show significant intermolecular hydrogen bonding interactions

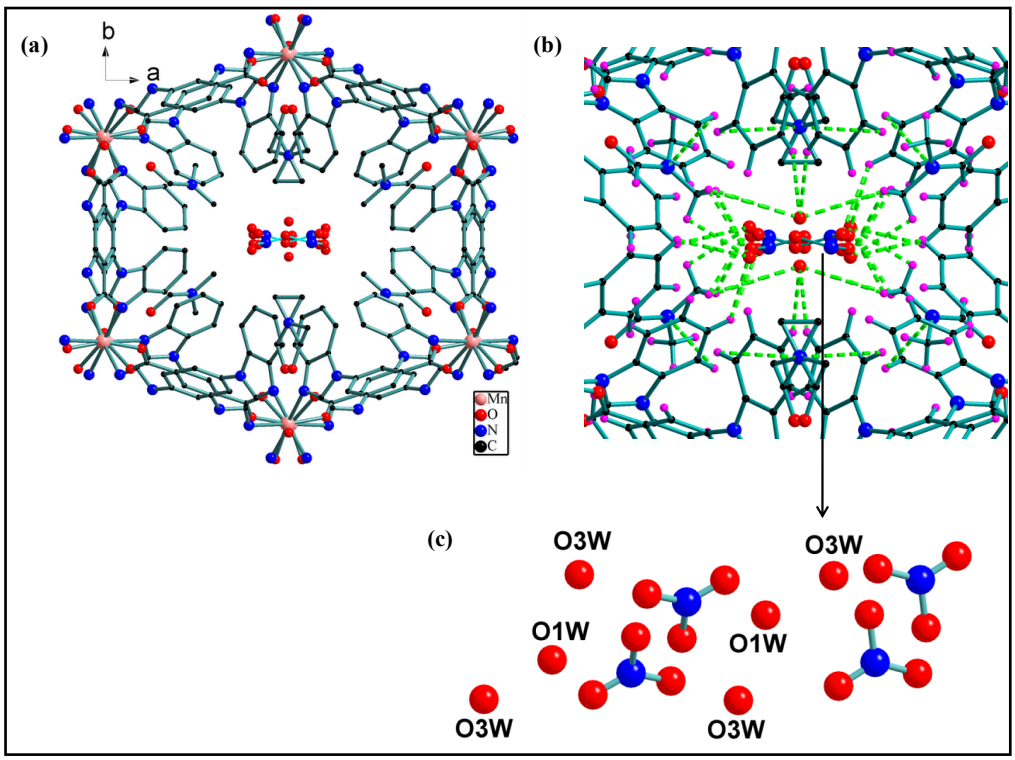

Figure 2 (a) View along *c* axis showing location of distorted DMF molecules and nitrate anion, (hydrogen atoms are omitted because of clarity) (b) intermolecular hydrogen bonding of framework with the guest water and DMF molecules and (c) a perspective view of the central part of cavity.

with the benzene rings of benzimidazole and hydrogen of methyl group of DMF. Nitrogen atoms of DMF molecule are also involved in hydrogen bonding with benzene ring hydrogens (Figure 2b).

An examination of the packing diagram of **1** along crystallographic *c* axis shows the existence of strong hydrogen bonding between nitrate anions, and water molecules (Figure 3).

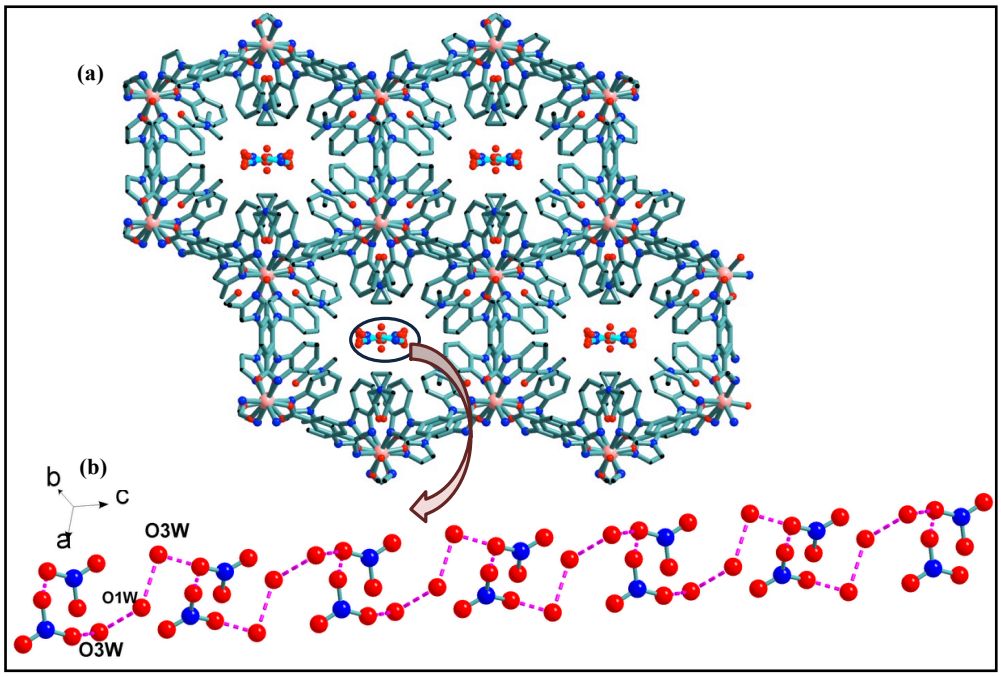

Figure 3 (a) Packing diagram of **1** along *c* axis and (b) central unit showing strong hydrogen bonding channel.

The solvent accessible volume is ~28.3 % of the unit cell volume, calculated from the crystal structure using the PLATON program.[22] (Figure S6).

Thermogravimetric analysis of **1** shows a weight loss of ~19% in the temperature range 35–290 ^{o}C, which corresponds to the loss of four water molecules and three DMF molecules (calcd 19.1%). After 370 ^{o}C the complex starts decomposing (Figure S7).

Gas adsorption studies

Gas adsorption measurements for N_2, H_2, and CO_2 gases were performed in a relative pressure range from 10^{-4} to 1 atm at 77 K (N_2 and H_2) and 195 K (CO_2) using activated compound prepared from **1**. Interestingly, the activated compound presented differential adsorption behaviour towards CO_2 (195 K), as compared to those for N_2 (77 K) and H_2 (77 K). The CO_2-sorption profile was of typical type-I nature with a significant uptake amount of 155 mL g^{-1} at 195 K, whereas both the N_2 and H_2-sorption plots refer to typical type-III nature (with negligible gas-uptake excluding the high-pressure induced surface adsorption at P/P_0>0.87)

(Figure 4). Here, size selective uptake can certainly be ruled out because of the bigger pore size compared to the kinetic diameters of the probe-adsorptive gas species (CO_2 = 3.3 Å, N_2 = 3.64 Å and H_2 = 2.8 Å).[23]

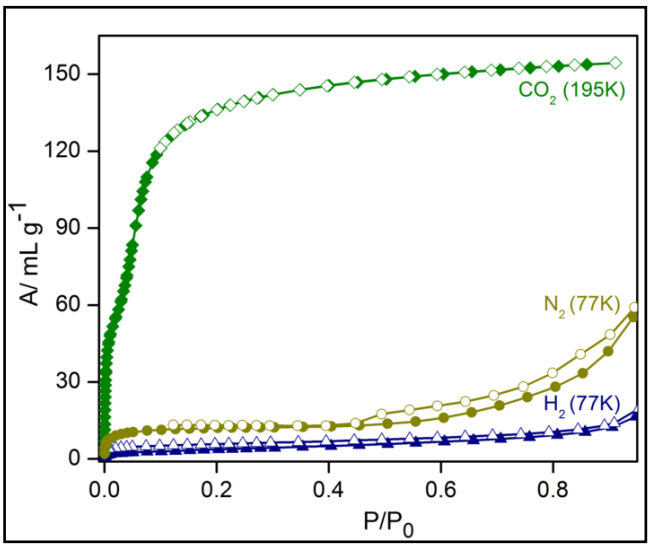

Figure 4 Low temperature gas-adsorption profiles for **1**, amount adsorbed (in mL g^{-1}) plot against P/P_0. (Filled shapes = adsorption, hollow shapes = desorption).

The type-III adsorption plots for N_2 and H_2 suggests of a notably weak interaction between the sample surface of **1** and these adsorbate gas molecules possessing zero dipole moment. On the contrary CO_2, having much larger quadruple moment (1.34 x 10^{-39} Cm^2), known to interact selectively with polar functionalities as compared to other gases registers a much higher adsorption-uptake with type-I profile, characteristic of strong interaction and also confirming the microporous nature of **1**. This striking low-temperature CO_2-selectivity further prompted to investigate the sorption performances for this material at room temperature (298 K), since the CO_2-adsorption amount at 273 K was experimentally found to be substantially high (73 mL g^{-1}) (Figure 5). The uptake amounts for all the four gaseous probe species, namely; CO_2, N_2, H_2 and CH_4 could evidently present CO_2-selective adsorption phenomena even at room temperature, since the amounts adsorbed were 50 mL g^{-1} for CO_2, 14.6 mL g^{-1} for N_2, 23 mL g^{-1} for CH_4 and 3 mL g^{-1} for H_2 (Figure 6).

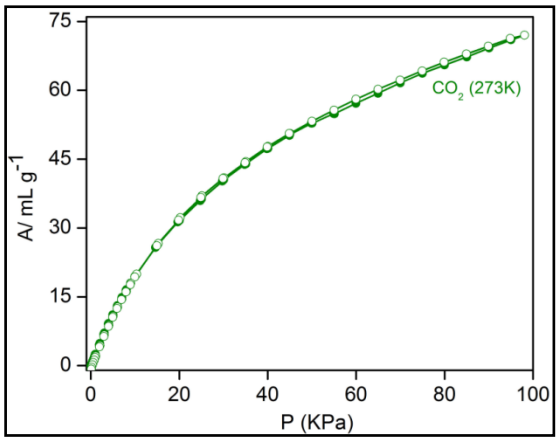

Figure 5 CO_2 sorption isotherm at 273 K for **1**. (Filled shapes = adsorption, hollow shapes = desorption).

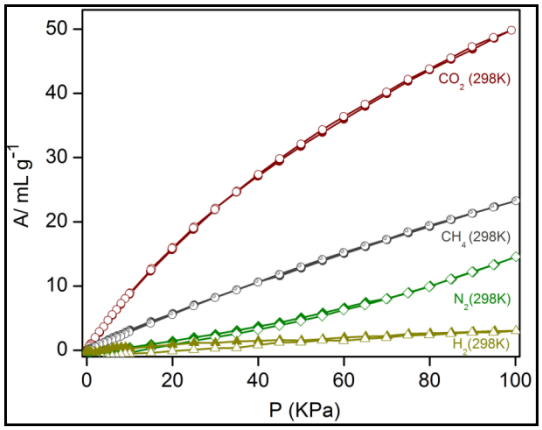

Figure 6 Adsorption isotherms of different gases (CO_2, CH_4, N_2 and H_2) at 298 K for **1**. (Filled shapes = adsorption, hollow shapes = desorption).

Since the adsorption amounts of other gases (H_2, N_2 and CH_4) are much smaller compare to CO_2, the compound **1** can prove expedient for separation of CO_2 from gas mixture at low to ambient temperature range. The CO_2/H_2 selectivity can be exploited in pre-combustion CCS (carbon capture and storage) technology, while The CO_2/N_2 selectivity makes it a prospective candidate for application in post-combustion CCS technology. BET Surface area as calculated from CO_2 adsorption isotherm at 195 K was found to be 365.82 $m^2\ g^{-1}$. The H-K (Haworth-Kawazoe) plot for CO_2 sorption at 195 K (Figure S8) reveals an effective pore diameter of 8.4 Å, which is relatively larger than kinetic diameter for any of the probe gases. This further confirms the fact that size-selectivity between different probe gases is not the deciding factor;

rather the selective uptake of CO_2 by **1** can be ascribed to the electrostatic interactions of CO_2 with nitrate anions and the carboxylate oxygens of the coordinated ligand.

The isosteric heat of adsorption for CO_2 is found to be 27.4 kJ/mol for low loading (Figure S9), as measured from CO_2-adsorption data plots at 273 K and 298 K. Phase purity of the sample was proved by PXRD measurements before and after activation (Figure S10). After activation, framework is devoid of any guest molecules.

Magnetic susceptibility data at an applied dc field of 0.3 T for **1** were collected in the 2–300 K temperature range. The plots of χT vs T and χ vs T are shown in Figure 7. The χT product has values of 9.16 cm^3 K mol^{-1} at 300 K. The observed value is slightly higher than that expected for two non-interacting Mn(II) ions with g = 2.0 and S = 5/2, of 4.375 x 2 = 8.75 cm^3 K mol^{-1}. As the temperature decreases, the χT product declines slightly, due to the Boltzmann depopulation of the excited states and simultaneous population of the antiferromagnetically coupled ground state. A maximum is observed in the χ versus T plot, indicating the population of and S = = spin ground state below the maximum T of 17 K.

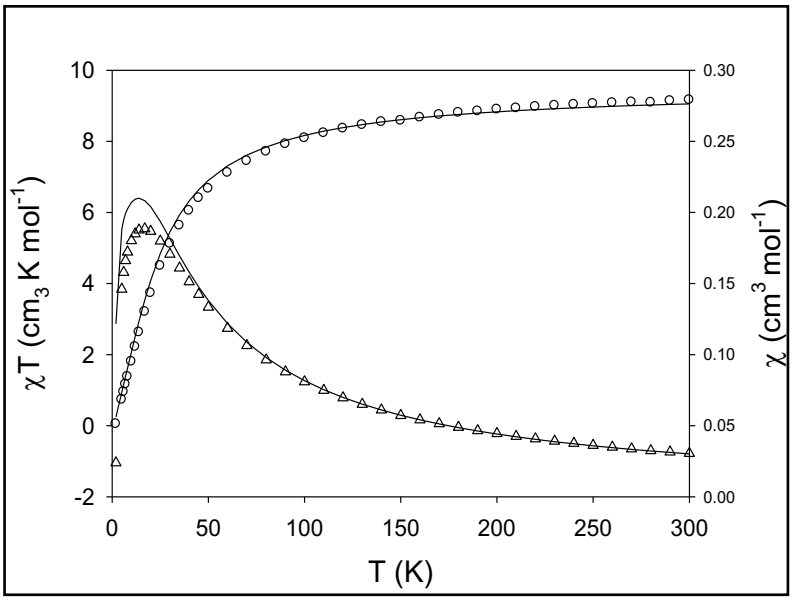

Figure 7 χT versus T (circles) and χ versus T (triangles, right axis) plots for **1** at an applied dc field of 0.3 T. The solid lines are the best fitting to a simplified model (see text for fitting parameters)

There are three well-defined structural motifs for **1**, which will have a great influence in the magnetic property. First, the binuclear Mn(II) unit is bridged by three *syn-syn* carboxylate groups with a distorted configuration (Figure 8), which are bent with torsion angles Mn-O-C-O'-Mn' between 60° and 70°. The lack of planarity will affect the super-exchange process through the delocalized π orbitals of carboxylate group, making it less effective and weaker. The second structural motif is, the unique arrangement of chains assembled by *meta-bis*-imidazole phenyl groups, constituted from the linking of the binuclear units (as presented in Figure 8).

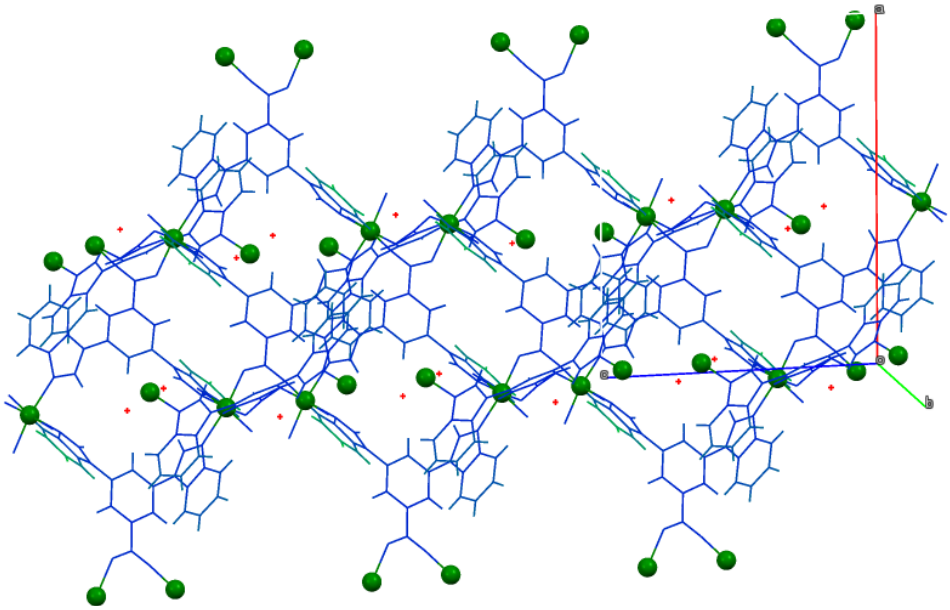

Figure 8 Simplified view along *c* axis of the unit cell, showing the way Mn_2 units (in green) are linked by the ligand (shown in blue). (The Mn-Mn distance within the binuclear unit is 4.0 Å, and between binuclear units 10.0 Å)

It is known, that this type of *meta*-substituted phenyl rings can lead to weak ferromagnetic coupling, although this is unlikely with Mn(II).[24] Finally as shown in Figure 3a, each one of these chains is a node in the basic hexagonal network.

The susceptibility and magnetization data were fitted together using the software package PHI.[25] PHI is a computer package designed for the calculation and interpretation of the magnetic properties of paramagnetic compounds which uses a phenomenological

Hamiltonian. This system is solved by evaluating the matrix elements of the Hamiltonian over the basis states and diagonalizing the Hamiltonian matrix. The model used to fit the magnetic data considers that the magnetic binuclear Mn(II) units of **1** are isolated. This is based on the crystal structure of **1** which shows Mn-Mn intranuclear distance is 4.0 Å and distance between the binuclear clusters is 10.0 Å. Taking into account that Mn(II)-Mn(II) couplings are very weak, the best fits are shown as solid lines in Figures 7 and S11. The best fitting parameters are g = 2.24 and J = -1.67 cm^{-1}. The deviation observed in the susceptibility plot at low temperatures can be attributed to the fact that inter-dimer interactions are not taken into account in the model, but these can be important at low temperature especially in a MOF where they propagate through the crystal.

In the crystal structure of **1**, nitrate anions, DMF and water molecules are involved in significant hydrogen bonding interactions with the framework, rendering the framework an ideal candidate for performing anion/solvent exchange studies. A crystal of **1** of suitable size is dipped in 3 M aqueous solution of $NaClO_4$ for 7 days at room temperature. It leads to complete replacement of NO_3^- with the ClO_4^- anion affording compound **2** with retention of crystallinity. A strong peak at 1,090 cm^{-1} in the IR spectrum of **2** suggests the presence of free ClO_4^- anion, (Figure S12). Similarly, when a crystal of **1** is dipped in 3 M aqueous solution of NaCl for 7 days at room temperature, complete replacement of NO_3^- by Cl^- occurs to afford compound **3** with retention of crystallinity. This is further supported by the IR spectra where complete disappearance of the NO_3^- peak at 1350 cm^{-1} suggests conversion of **1** into **3** (Figure S13). Likewise, compounds **4** and **5** can be obtained from **1** in SCSC fashion by dipping a crystal of **1** in dry methanol and dry acetone respectively. The IR spectra of **4** and **5** are indicative of the presence of methanol (Figure S14) and acetone (Figure S15) respectively. Snapshots were taken before and after each SCSC transformation reaction (Figure S16).

However, in each case of these SCSC transformation reactions, the crystal quality is maintained there is no change in colour and shape.

Crystallographic space group of **1** underwent a clear change from monoclinic *C*2/*c* to triclinic *P*-1, in both **2** and **3.** For compound **2**, when viewed along the *c* axis, two perchlorate anions which are opposite to each other in a single cavity remain sandwiched between two benzene rings of different benzimidazole moieties; while in **3**, the chloride ions are present between binuclear cluster units along the *a* axis (Figure 9). Both π–π and anion–π interactions are present in the hexagonal cavity. In **3**, a view along the *b* axis shows chloride ions to be involved in hydrogen bonding interactions with the central benzene ring of the ligand (Figure 10), but no such hydrogen bonding interactions is present in **2** (Figure 11). In both the structures, metal to anion distance is decreased significantly compare to that of the framework **1**.

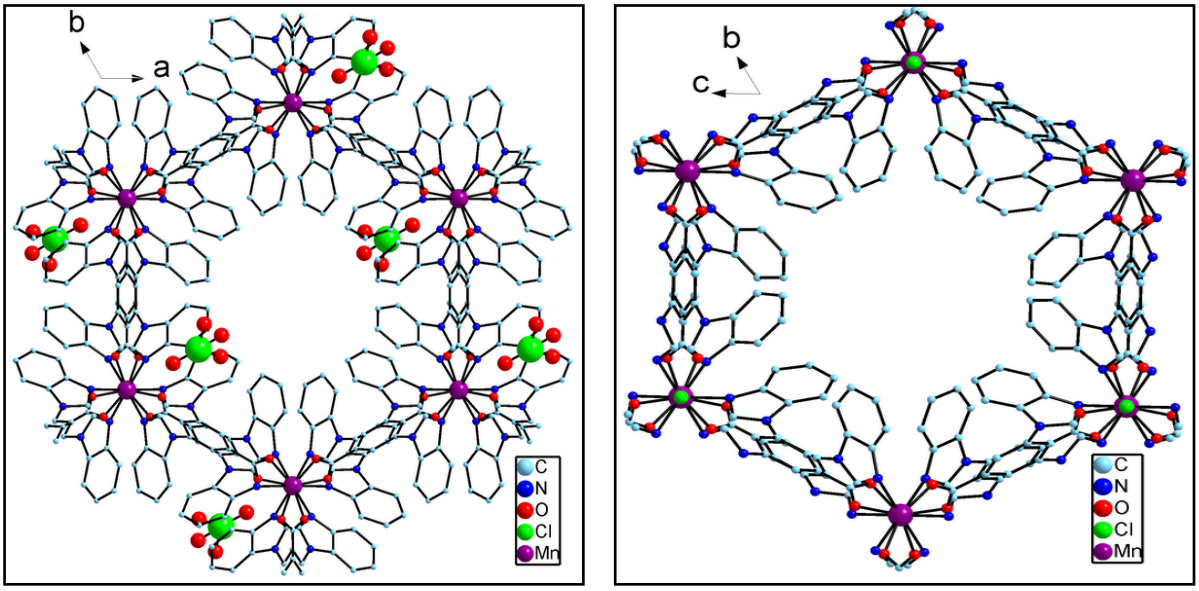

(a) (b)

Figure 9 (a) View along the *c* axis showing perchlorate anions in **2** and (b) view along the *a* axis showing chloride anions in **3**.

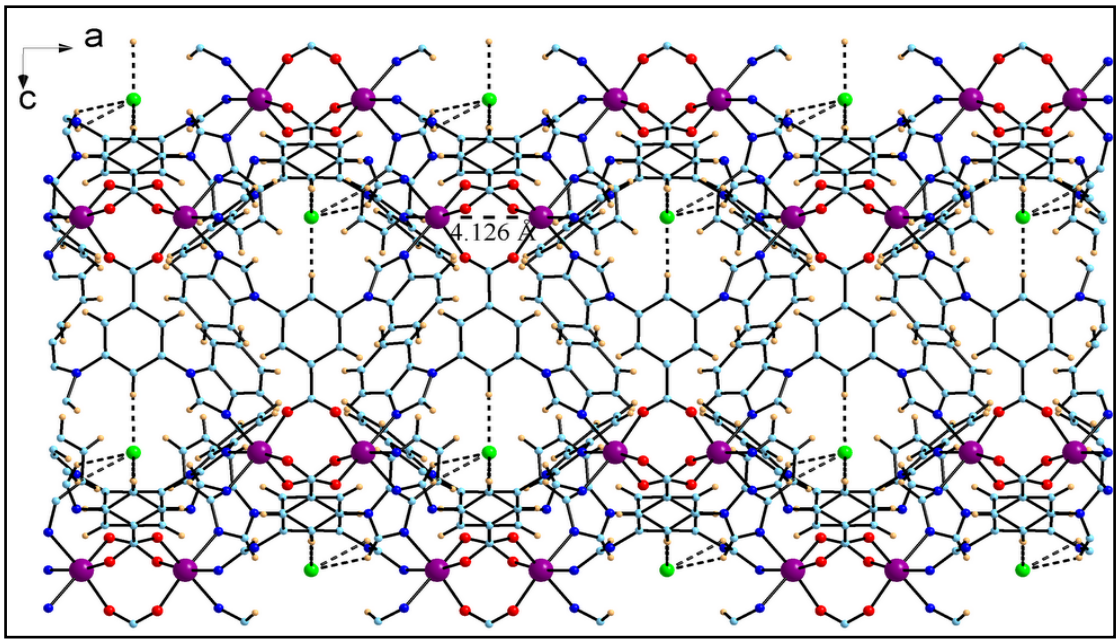

Figure 10 Showing hydrogen bonding interactions of chloride ions with the framework along *b* axis in **3**.

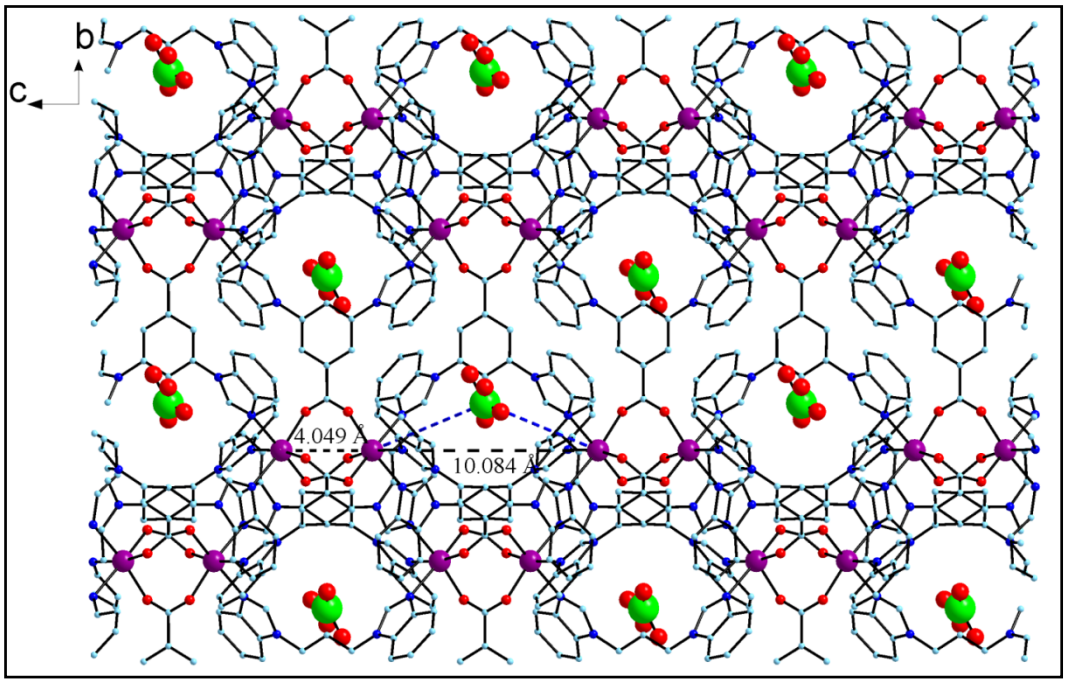

Figure 11 View along *a* axis showing perchlorate anions in **2**.

The solvent accessible volume in **3** is increased up to ~34% of the unit cell volume (Figure 12), calculated from the crystal structure using the PLATON program [22].

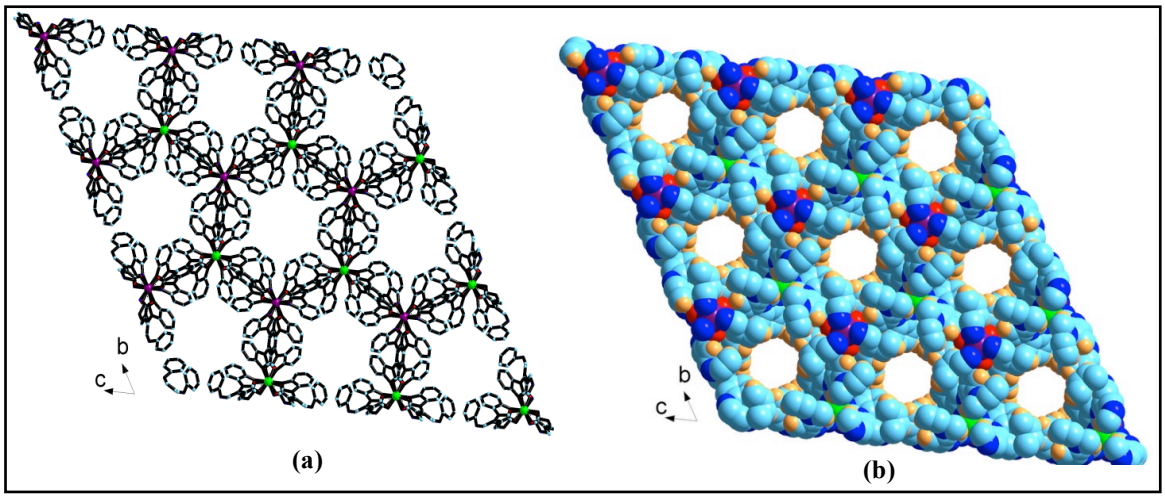

Figure 12 Packing diagram of **3** (a) ball and stick model and (b) space fill model.

Interestingly, the crystal system changed to trigonal (*P*-31*c*) in case of **4** and triclinic (*P*-1) in case of **5**. Bond distances involving the metal ions in **4** are slightly changed in comparison to complex **1** (Figure 13).

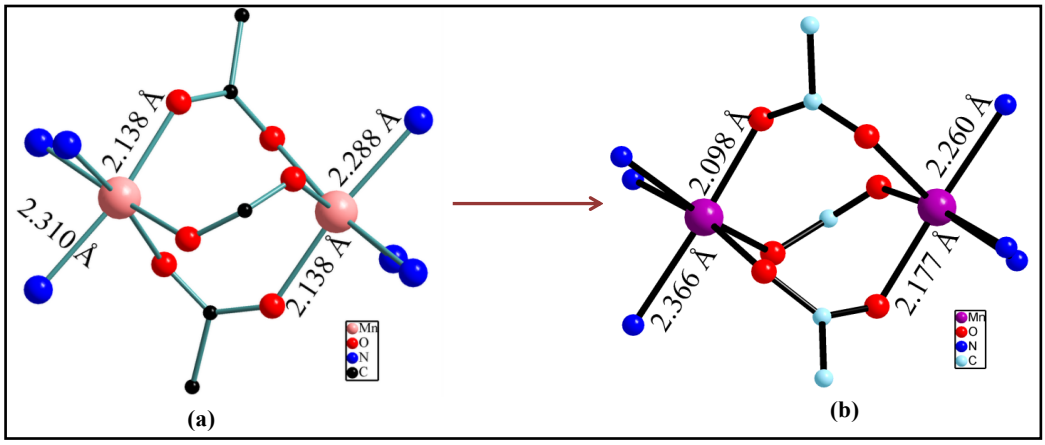

Figure 13 Binuclear cluster showing bond distances in (a) **1** and (b) **4**.

Also, unlike in **1**, no appreciable π–π interactions can be observed between benzene rings of benzimidazole in **4** after methanol inclusion (Figure 14), while strong π–π interactions are present in **5** along the *a* axis (Figure 15). Metal to anion distance gets decreased in case of **4** and the anion NO_3^- is placed between two binuclear clusters revealing strong hydrogen bonding with the hydrogens of imidazole moiety and central benzene ring of the ligand (Figure 16). Metal to anion distance gets increased in **5** in comparison to **1** and anion is located between

two benzimidazoles of two different ligands, and oxygen atom of acetone molecule is involved in hydrogen bonding interaction with hydrogen of central benzene ring (Figure 17).

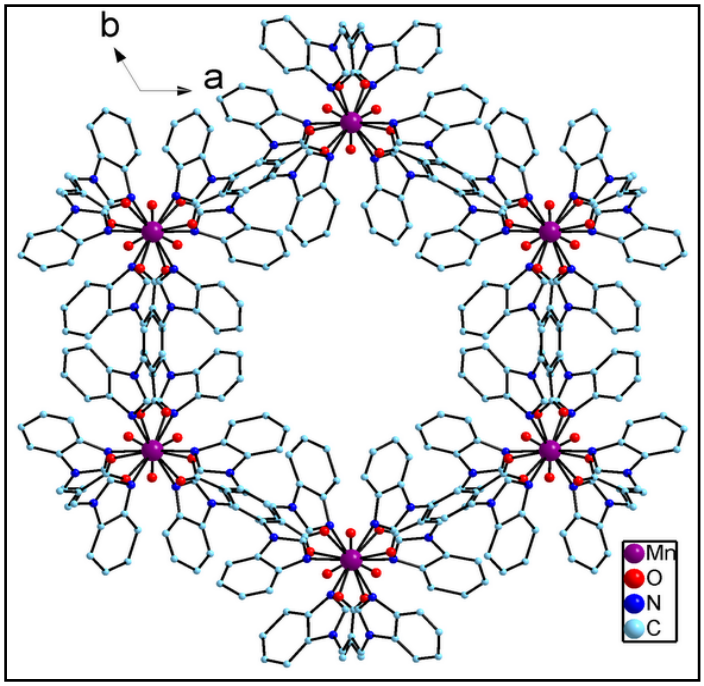

Figure 14 View along *c* axis showing no π–π interactions in cavity of **4**.

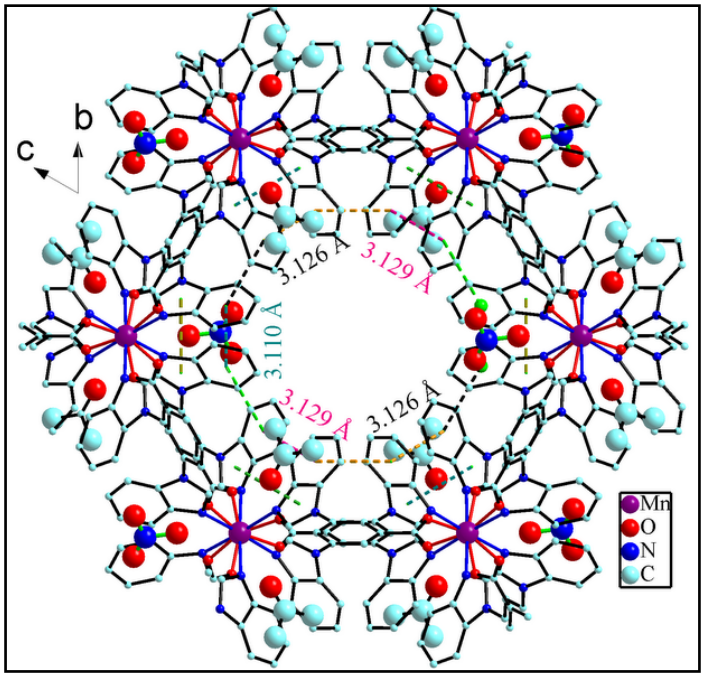

Figure 15 Strong π–π interactions along *a* axis in cavity of **5**.

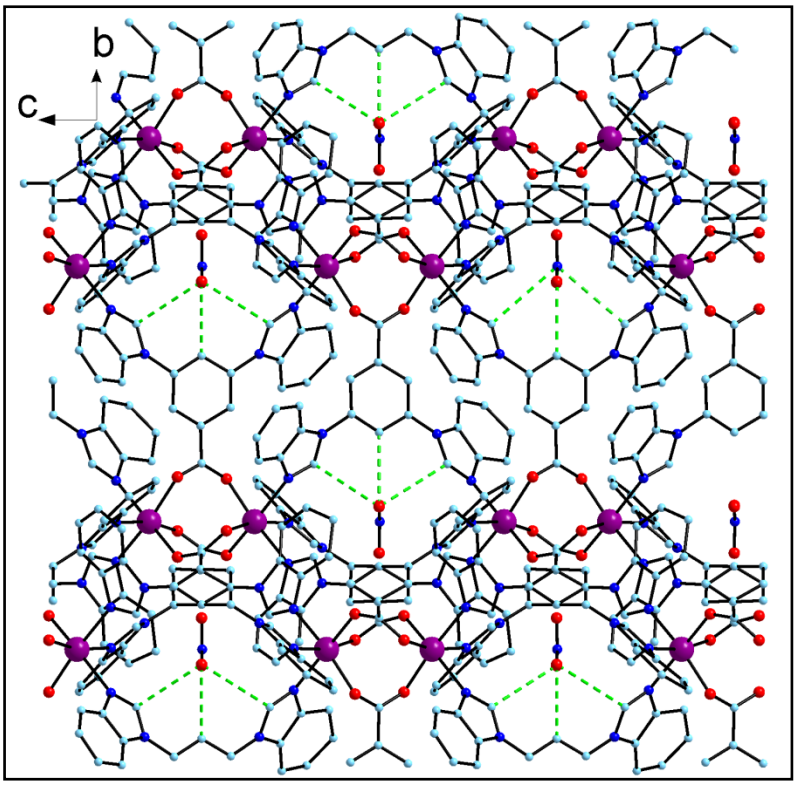

Figure 16 Hydrogen bonding between nitrate anion and the framework in **4**.

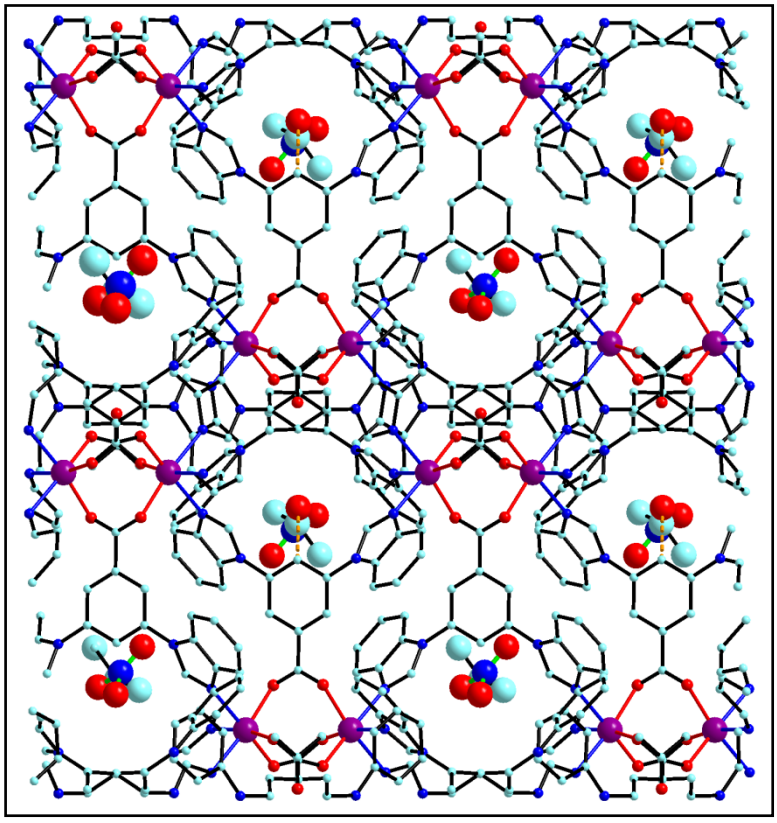

Figure 17 Involvement of acetone molecules in hydrogen bonding with the framework in **5**.

The solvent accessible volume in **4** is increased to ~33.6% (Figure S17), while in **5** it remains almost constant as in **1**.

Guest-exchange reactions were monitored by powder X-ray diffraction technique. The similar PXRD patterns observed for the exchanged products are indicative of the fact that the entire framework is retained, throughout the SCSC transformations mediated by solvent and anion-exchange processes (Figure 18).

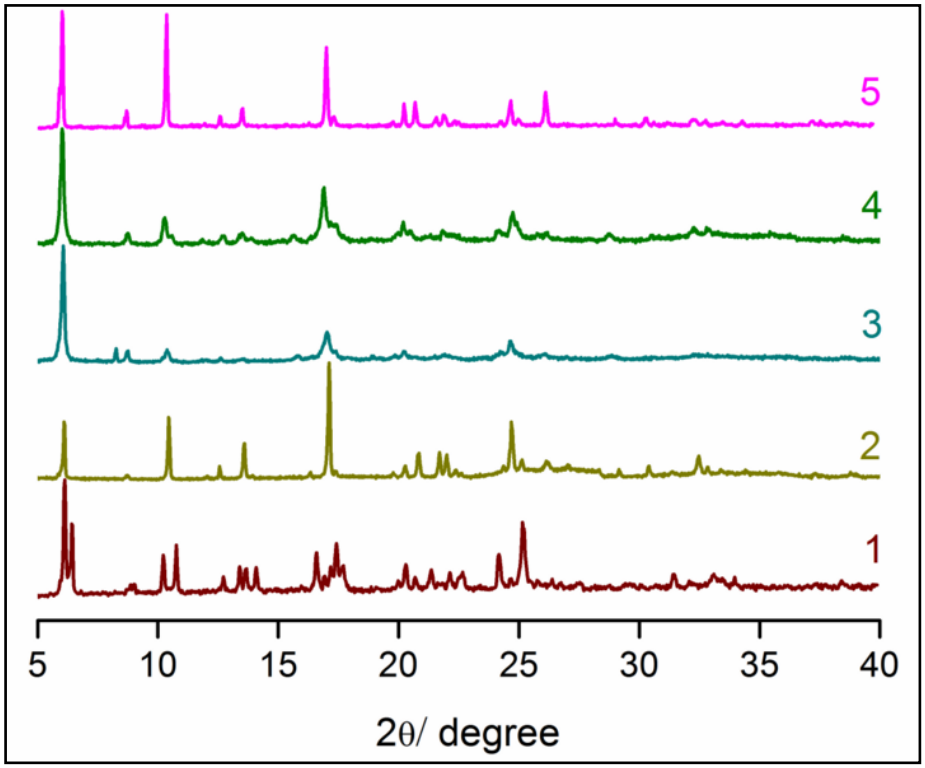

Figure 18 PXRD patterns for **1-5** complexes.

All the key parameters which have been altered during the guest exchange reactions have been summarized in the form of Tables 3 and 4.

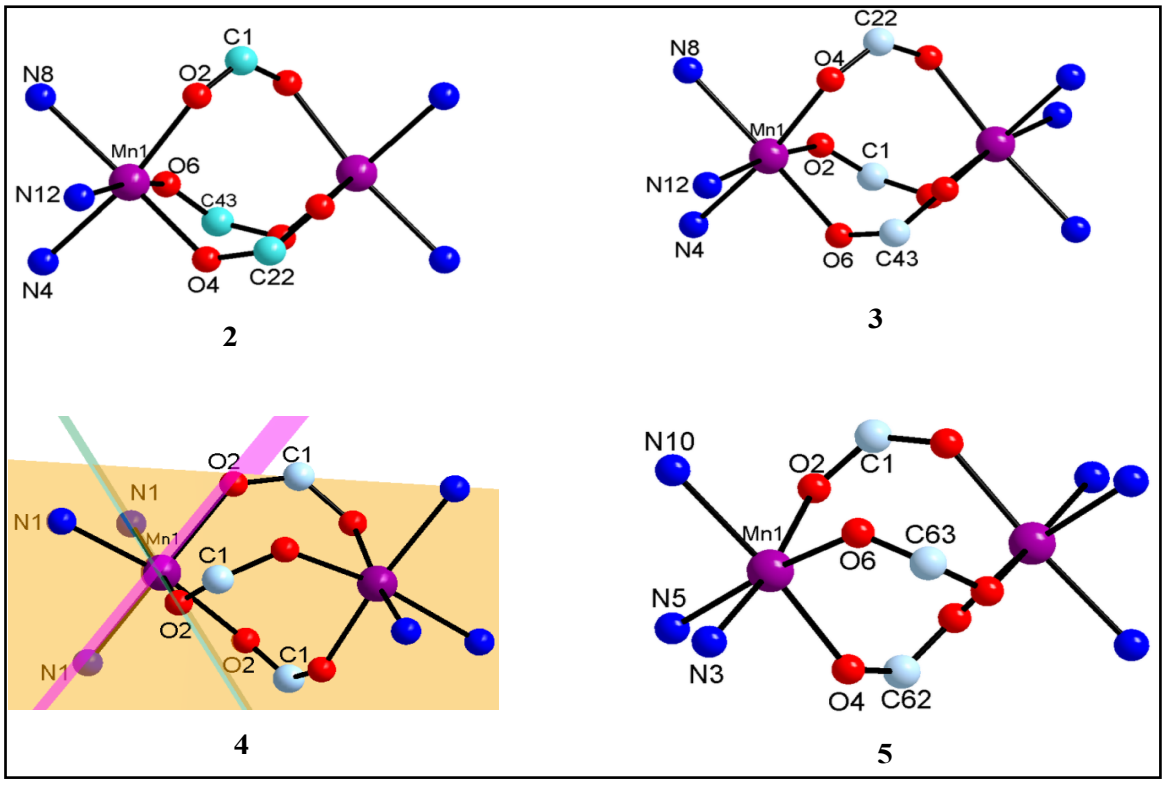

Figure 19 Planes and labeled atoms in binuclear clusters of **2** to **5**.

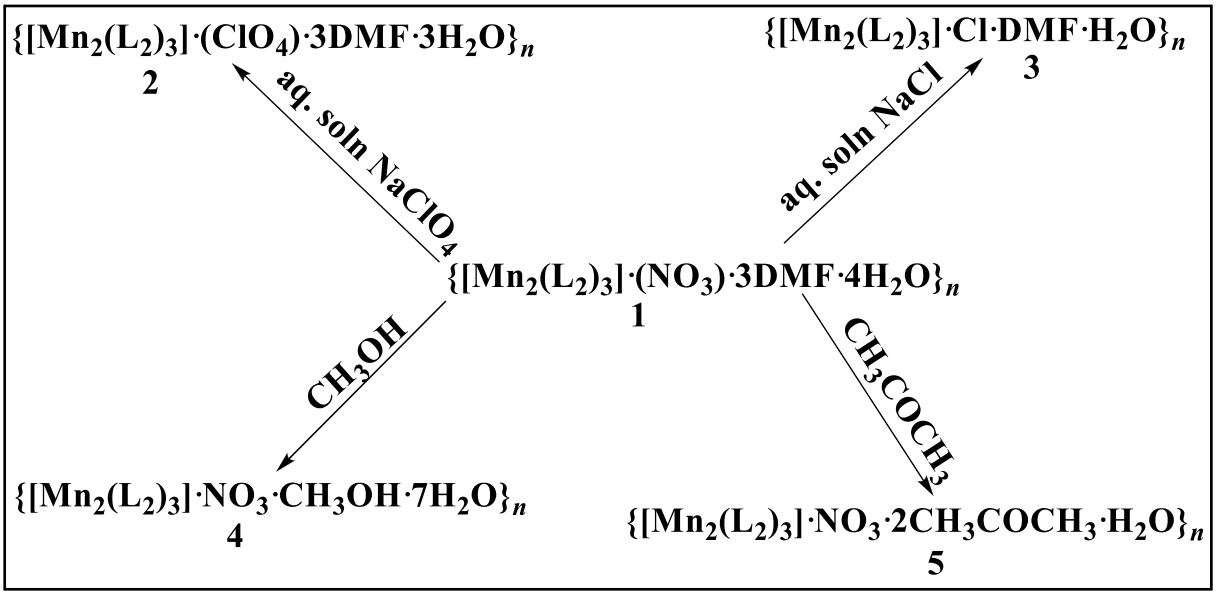

Scheme 2 Schematic representation of guest exchange within the channels of **1**

Conclusion

In summary, a new 3D coordination polymer of Mn(II) (**1**) have been synthesized displaying anion/solvent exchange mediated development of four analogous isostructural

coordinaton polymers (**2**-**5**) in single-crystal to single-crystal (SCSC) fashion, with precise crystalline framework-retention during which supramolecular non-covalent interactions play extremely crucial role. Guest-free activated phase of complex **1** exhibits the intriguing selective CO_2-sorption phenomena at low to ambient temperature and at low pressure regime. Magnetic measurements on **1** show that it also behaves as a weak antiferromagnetic material below 17 K.

Supporting Information X-ray crystallographic data in CIF format, table for selected bonds and distances for **1**–**5**, IR, TGA and PXRD analysis. This material is available free of charge via the internet at http://pubs.acs.org/.

Acknowledgement. PKB gratefully acknowledges the financial support received from the Department of Science and Technology, New Delhi, India. ECS acknowledges the financial support from the Spanish Government, (Grant CTQ2012-032247 and Ramón y Cajal contract). SM acknowledges IISER Pune for research facilities and funding.

Reference

1. (a) Yaghi, O. M.; Li, H. *J. Am. Chem. Soc.* **1995**, *117*, 10401. (b) Kamiyama, A.; Noguchi, T.; Kajiwara, T.; Ito, T. *Angew. Chem.,Int. Ed.* **2000**, *39*, 3130.

2. (a) Uemura, K.; Kitagawa, S.; Kondo, M.; Fukui, K.; Kitaura, R.; Chang, H.-C.; Mizutani, T. *Chem. Eur. J*. **2002**, *8*, 3587. (b) Ahmad, M.; Bharadwaj, P. K. *Polyhedron,* **2013,** *42, 1145.*

3. (a) Rosi, N. L.; Eckert, J.; Eddaoudi, M.; Vodak, D. T.; Kim, J.; 'Keeffe, M.; Yaghi, O. M. *Science* **2003**, *300*, 1127. (b) Noro, S.; Kitagawa, S.; Kondo, M.; Seki, K. *Angew. Chem., Int. Ed*. **2000**, *39*, 2081. (c) Sahu, R.; Ahmad, M.; Bharadwaj, P. K. *Cryst. Growth Des*, **2013**, *13*, 2618. (d) Singh, R.; Ahmad, M.; Bharadwaj, P. K. *Cryst. Growth Des*, **2012**, *12*, 5025.

4. (a) Halder, G. J.; Kepert, C. J.; Moubaraki, B.; Murray, K. S.; Cashion, J. D. *Science* **2002**, *298*, 1762. (b) Ahmad, M.; Sharma, M. K.; Das, R.; Poddar, P.; Bharadwaj, P. K. *Cryst. Growth Des.* **2012**, *12*, 1571. (c) Ahmad, M.; Das, R.; Lama, P.; Poddar, P.; Bharadwaj, P. K. *Cryst. Growth Des*, **2012**, *12*, 4624. (d) Ahmad, M.; Katoch, R.; Garg, A.; Bharadwaj, P. K. *CrystEngComm.* **2014**, *16*, 4766.
5. Maspoch, D.; Ruiz-Molina, D.; Wurst, K.; Domingo, N.; Cavallini, M.; Biscarini, F.; Tejada, J.; Rovira, C.; Veciana, J. *Nature Mat.* **2003**, *2*, 190.
6. Gallo, M.; Glossnan-Mitnik, D. *J. Phys. Chem.* C **2009**, *113*, 6634.
7. (a) Kitaura, R.; Seki, K.; Akiyama, G.; Kitagawa, S. *Angew. Chem., Int. Ed.* **2003**, *42*, 428. (b) Chen, B.; Ma, S.; Zapata, F.; Fronczek, F. R.; Lobkovsky, E. B.; Zhou, H.-C. *Inorg. Chem.* **2007**, *46*, 1233.
8. Millward, A. R.; Yaghi, O. M. *J. Am. Chem. Soc.* **2005**, *127*, 17998.
9. (a) Waldo, G. S.; Yu, S.; Penner-Hahn, J. E. *J. Am. Chem. Soc.* **1992**, *114*, 5869. (b) Tan, X. S.; Xiang, D. F.; Tang, W. X.; Sun, J. *Polyhedron* **1997**, *16*, 689. (c) Policar, C.; Lambert, F.; Cesario, M.; Morgenstern-Badarau, I. *Eur. J. Inorg. Chem.* **1999**, 2201. (d) Delgado, F. S.; Kerbellec, N.; Ruiz-Perez, C.; Cano, J.; Lloret, F.; Julve, M. *Inorg. Chem.* **2006**, *45*, 1012.
10. (a) Meng, M.; Zhong, D.-C.; Lu, T. B. *CrystEngComm*. **2011**, *13*, 6794. (b) Lampropoulos, C.; Redler, G.; Data, S.; Abboud, K. A.; Hill, S.; Christou, G. *Inorg. Chem*. **2010**, *49*, 1325. (c) Berggren, G.; Huang, P.; Eriksson, L.; Styring, S.; Anderlund, M. F.; Thapper, A. *Dalton Trans*. **2010**, *39*, 11035. (d) Li, Y.; Zou, W. Q.; Wu, M. F.; Lin, J. D.; Zheng, F. K.; Liu, Z. F.; Wang, S. H.; Guo, G. C.; Huang, J. S. *CrystEngComm* **2011**, *13*, 3868.
11. (a) Wang, Y. Q.; Sun, Q.; Yue, Q.; Cheng, A. L.; Song, Y.; Gao, E. Q. *Dalton Trans*. **2011**, *40*, 10966. (b) Wang, X. F.; Zhang, Y. B.; Zhang, W. X.; Xue, W.; Zhou, H. L.; Chen, X. M. *CrystEngComm* **2011**, *13*, 4196. (c) Ma, C. B.; Hu, M. Q.; Chen, H.; Wang, M.; Zhang,

C. X.; Chen, C. N.; Liu, Q. T. *CrystEngComm* **2010**, *12*, 1467. (d) Chen, W. X.; Zhuang, G. L.; Zhao, H. X.; Long, L. S.; Huang, R. B.; Zheng, L. S. *Dalton Trans*. **2011**, *40*, 10237.

12. Janiak, C. *Dalton Trans.* **2003**, 2781.
13. (a) Coronado, E.; Palacio, F.; Veciana, J. *Angew. Chem*. **2003**, *115*, 2674; *Angew. Chem. Int. Ed*. **2003**, *42*, 2570. (b) Day, P.; Underhill, A. E. "Metal-Organic and Organic Molecular Magnets": *Philos. Trans. R. Soc. London, Ser. A* **1999**, *357*, 2849. (c) Kahn, O. Molecular Magnetism, VCH, New York, **1993**.
14. (a) Zhou, X. P.; Zhang, X. J.; Lin, S. H.; Li, D. *Cryst. Growth Des.* **2007**, *7*, 485. (b) Jung, O. S.; Park, S. H.; Kim, K. M.; Jang, H. G. *Inorg. Chem*. **1998**, *37*, 5781. (c) Withersby, M. A.; Blake, A. J.; Champness, N. R.; Cooke, P. A.; Hubberstey, P.; W. S. Li, M. Schröder, *Inorg. Chem.* **1999**, *38*, 2259. (d) Chen, H. B.; Zhang, H.; Yang, J. M.; Zhou, Z. H. *Polyhedron* **2004**, *23*, 987.
15. (a) Sun, W. Y.; Fan, J.; Okamura, T. A.; Xie, J.; Yu, K. B.; Ueyam, N. *Chem. Eur. J.* **2001**, *7*, 2557. (b) Fan, J.; Gan, L.; Kawaguchi, H.; Sun, W. Y.; Yu, K. B.; Tang, W. X. *Chem. Eur. J.* **2003**, *9*, 3965.(c) Liu, H. K.; Huang, X. H.; Lu, T. H.; Wang, X. J.; Sun, W. Y.; Kang, B. S. *Dalton Trans*. **2008**, 3178.
16. (a) Reger, D. L.; Semeniuc, R. F.; Rassolov, V.; Smith, M. D. *Inorg. Chem*. **2004**, *43*, 537. (b) Sarkar, M.; Biradha, K. *Cryst. Growth Des*. **2006**, *6*, 1742. (d) Dalrymple, S. A.; Shimizu, G. K. H. *Chem. Eur. J.* **2002**, *8*, 3010. (c) Qiu, Y. C.; Liu, Z. H.; Li, Y. H.; Deng, H.; Zeng, R. H.; Zeller, M. *Inorg. Chem.* **2008**, *47*, 5122. (d) Wang, Y.; Cheng, P.; Song, Y.; Liao, D. Z.; Yan, S. P. *Chem. Eur. J.* **2007**, *13*, 8131. (e) Xu, G. C.; Ding, Y. J.; Huang, Y. Q.; Liu, G. X.; Sun, W. Y. *Microporous Mesoporous Mater.* **2008**, *113*, 511.
17. Kitagawa, S.; Matsuda, R. *Coord. Chem. Rev*. **2007**, *251*, 2490.
18. (a) Nouar, F. N.; Eubank, J. F.; Bousquet, T.; Wojtas, L.; Zaworotko, M. J.; Eddaoudi, M. *J. Am. Chem. Soc*. **2008**, *130*, 1833. (b) Lan, Y. Q.; Li, S. L.; Shao, K. Z.; Wang, X. L.;

Du, D. Y.; Su, Z. M.; Wang, D. J. *Cryst. Growth Des*. **2008**, *8*, 3940. (c) Zhai, Q. G.; Wu, X. Y.; Chen, S. M.; Zhao, Z. G.; Lu, C. Z. *Inorg. Chem*. **2007**, *46*, 5046. (d) Singh, R.; Bharadwaj, P. K. *Cryst. Growth Des*, **2013**, *13*, 3722. (e) Singh, R.; Mrozenski, J.; Bharadwaj, P. K. *Cryst. Growth Des*, **2014**, ***DOI:*** 10.1021/cg5005775.

19. König, E. Magnetic Properties of Coordination and Organometallic Transition Metal Compounds, Springer, Berlin, **1966**.
20. Agarwal, R. A.; Aijaz, A.; Ahmad, M.; Sañudo, E. C.; Xu, Q.; Bharadwaj, P. K. *Cryst. Growth Des.* **2012**, *12*, 2999.
21. Agarwal, R. A.; Aijaz, A.; Sañudo, E. C.; Xu, Q.; Bharadwaj, P. K. *Cryst. Growth Des.* **2013**, *13*, 1238.
22. Spek, A. L. *PLATON*; The University of Utrecht: Utrecht, The Netherlands, **1999**.
23. (a) Férey, G.; Serre, C.; Devic, T.; Maurin, G.; Jobic, H.; Llewellyn, P. L.; Weireld, G. D.; Vimont, A.; Daturi, M.; Chang, J.-S. *Chem. Soc. Rev.* **2011**, *40*, 550. (b) Nagarkar, S. S.; Chaudhari, A. K.; Ghosh, S. K. *Inorg. Chem*. **2012**, *51*, 572. (c) Chaudhari, A. K.; Mukherjee, S.; Nagarkar, S. S.; Joarder, B.; Ghosh, S. K. *CrystEngComm.* **2013**, *15*, 9465.
24. (a) Wang, J.; Bei, F. L.; Yang, X. J.; Lu, L. D.; Wang, X. *J. Mol. Struct*. **2002***, 643*, 129. (b) Laye, R. H.; Sañudo, E. C. *Inorg. Chim. Acta.* **2009***, 362*, 2205. (c) Paital, A. R.; Mitra, T.; Ray, D.; Wong, W. T.; Ribas-Ariño, J.; Novoa, J. J.; Ribasa, J.; Aromı, G. *Chem. Commun*. **2005**, 5172.
25. Chilton, N. F.; Anderson, R. P.; Turner, L. D.; Soncini, A.; Murray, K. S. *J. Comput. Chem.* **2013**, DOI: 10.1002/jcc.23234.

Table 1 Crystal and Structure Refinement Data for **1** to **3**

	1	**2**	**3**
Empirical formula	$C_{72}H_{68}N_{16}O_{16}Mn_2$	$C_{72}H_{66}N_{15}O_{16}ClMn_2$	$C_{66}H_{48}N_{13}O_8ClMn_2$
Formula wt.	1523.18	1542.39	1296.39
Crystal system	Monoclinic	Triclinic	Triclinic
Space group	*C* 2/*c*	*P*-1	*P*-1
a, Å	17.966(5)	17.105(5)	14.135(5)
b, Å	27.989(5)	17.108(5)	17.246(5)
c, Å	14.141(5)	14.133(5)	17.247(5)
α (°)	90.00	90.015	60.083(5)
β (°)	92.381	90.003	89.997(5)
γ (°)	90.00	119.988	89.975(5)
U, Å^3	7105(3)	3582.1(19)	3644(2)
Z	4	2	2
ρ_{calc} g/cm^3	1.410	1.177	1.099
μ, mm^{-1}	0.435	0.448	0.433
Temperature (K)	100	100	100
θ max	25.50	25.50	25.50
F(000)	3100	1296	1232
Refl. collected	19102	25195	22649
Independent refl.	4408	7517	4301
GOOF	1.036	0.953	1.096
Final R indices [$I>2\sigma(I)$]	*R*1 = 0.0789 w*R*2 = 0.1986	*R*1 = 0.0665 w*R*2 = 0.1719	*R*1 = 0.0982 w*R*2 = 0.2540
R indices (all data)	*R*1 = 0.1219 w*R*2 = 0.2360	*R*1 = 0.1130 w*R*2 = 0.1887	*R*1 = 0.2265 w*R*2 = 0.2745

Table 2 Crystal and Structure Refinement Data for **4** and **5**

Compound	**4**	**5**
Empirical formula	$C_{64}H_{57}N_{13}O_{17}Mn_2$	$C_{69}H_{53}N_{13}O_{12}Mn_2$
Formula wt.	1389.95	1366.11
Crystal system	Trigonal	Triclinic
Space group	*P*-31*c*	*P*-1
a, Å	17.485(5)	14.045(5)
b, Å	17.485(5)	17.203(5)
c, Å	14.019(5)	17.203(5)
α (°)	90.00	60.025(5)
β (°)	90.00	89.983(5)
γ (°)	120.000(5)	89.994(5)
U, Å^3	3712(2)	3601(2)
Z	2	2
ρ_{calc} g/cm^3	1.102	1.243
μ, mm^{-1}	0.395	0.415
Temperature (K)	100	100
θ max	25.49	25.48
F(000)	1260	1388
Refl. collected	20669	19841
Independent refl.	2805	5432
GOOF	0.958	0.899
Final R indices [$I>2\sigma(I)$]	$R1$ = 0.0566 w$R2$ = 0.1129	$R1$ = 0.0799 w$R2$ = 0.1685
R indices (all data)	$R1$ = 0.1024 w$R2$ = 0.1264	$R1$ = 0.1707 w$R2$ = 0.2062

Table 3 Key Parameters changed during guest exchange for **1** to **5**

Complexes	π–π bonding in cavity (Å)	Hydrogen bonding with anion (Å)	Metal to anion distance (Å)	Anion–π interaction (Å)

1	3.065–3.310	–	9.132–12.54	–
2	3.125–3.230	–	6.586–6.597	3.031–3.529
3	3.249–3.580	2.413–2.866	5.004–5.006	3.822–3.843
4	–	3.134–3.446	4.910–4.943	3.749
5	3.110–3.253	–	14.712–14.831	2.761–3.508

Table 4 Torsion and dihedral angles changed during guest exchange for **2** to **5**

Complexes	Torsion angles (º)	Dihedral angles (º) between following two planes passing through metal atom
2	N4 Mn1 O2 C1, N8 Mn1 O4 C22, N12 Mn1 O6 C43 = -76.05	N8 Mn1 O4 and N12 Mn1 O6 (76), N8 Mn1 O4 and N4 Mn1 O2 (76.8), N4 Mn1 O2 and N12 Mn1 O6 (76)
3	N8 Mn1 O6 C43 (-66.77), N12 Mn1 O2 C1 (-65.3), N4 Mn1 O4 C22 (-65.3)	N8 Mn1 O6 and N4 Mn1 O4 (69.16), N8 Mn1 O6 and N12 Mn1 O2 (65.8), N4 Mn1 O4 and N12 Mn1 O2 (66.47)
4	N1 Mn1 O2 C1 (-69)	N1 Mn1 O2 and N1 Mn1 O2 (65.6)
5	N10 Mn1 O4 C62 (76.26), N5 Mn1 O6 C63 (71.17), N3 Mn1 O2 C1 (80.19)	N10 Mn1 O4 and N5 Mn1 O6 (71.49), N10 Mn1 O4 and N3 Mn1 O2 (75.67), N5 Mn1 O6 and N3 Mn1 O2 (79)

Gas Adsorption, Magnetism and Single-Crystal to Single-Crystal Transformation Studies of a Three Dimensional Mn(II) Porous Coordination Polymer

Rashmi A. Agarwal,[a] *Soumya Mukherjee*,[b] *E. Carolina Sañudo*,[c] *Sujit K. Ghosh*[b] *and Parimal K. Bharadwaj*[a]*

[a]*Department of Chemistry, Indian Institute of Technology Kanpur, 208016, India*

[b] *Department of Chemistry, Indian Institute of Science Education and Research (IISER), Dr. Homi Bhabha Road, Pashan, Pune, Maharashtra 411021, India*

[c]*Departament de Quımica Inorganica, Universitat de Barcelona, Diagonal, 645, 08028-Barcelona, Spain*

For Table of Contents

A microporous coordination polymer of Mn(II) has been synthesized under solvothermal conditions that shows selective CO_2 sorption at low temperature and pressure. Four isostructural complexes are obtained through anion/solvent exchange reactions at room temperature in single-crystal to single-crystal (SCSC) pathway.

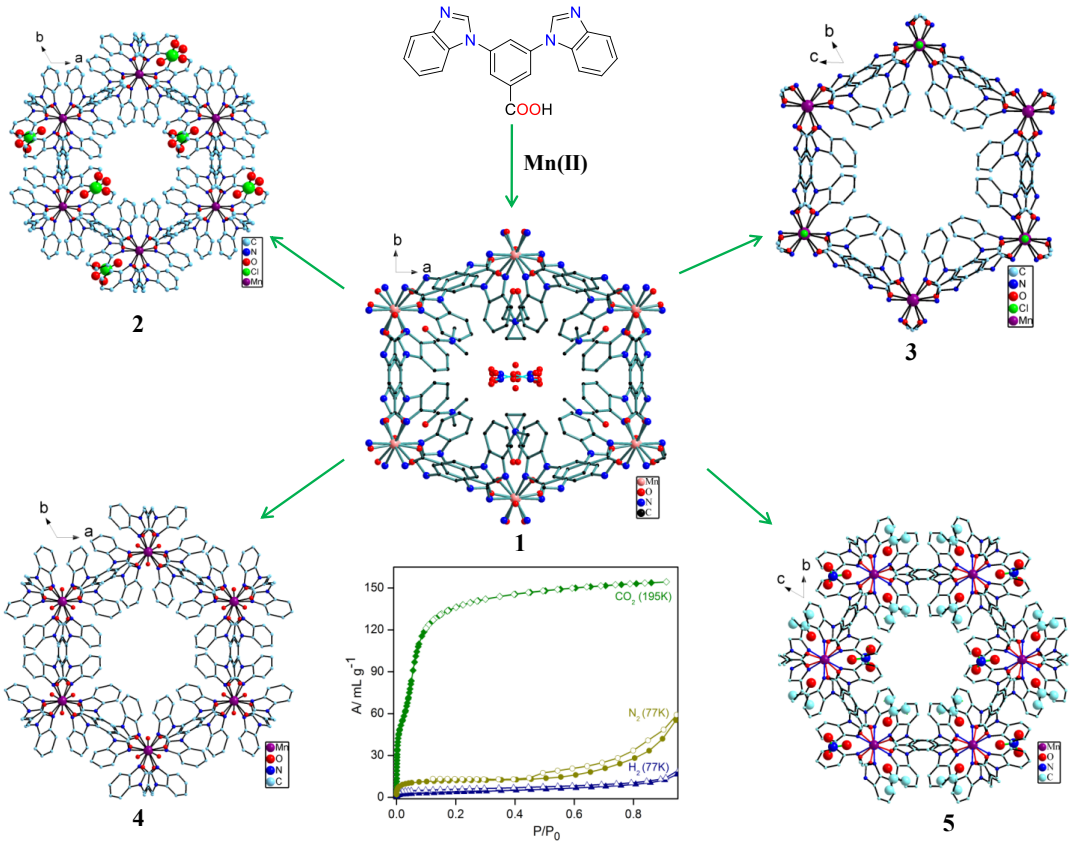
COOH
Mn(II)
1
2
3
4
5
CO2 (195K)
N2 (77K)
H2 (77K)
A/ mL g-1
P/P0